



Article

How often do Protein Genes Navigate Valleys of Low Fitness?

Erik D. Nelson^{1,*}  and Nick V. Grishin¹

¹ Howard Hughes Medical Institute, University of Texas Southwestern Medical Center, 6001 Forest Park Blvd., Room ND10.124, Dallas, Texas 75235-9050, USA

* Correspondence: nelsonerikd@gmail.com

Version March 28, 2019 submitted to *Genes*

Abstract: In order to escape from local fitness peaks, a population must navigate across valleys of low fitness. How these transitions occur, and what role they play in adaptation, have been subjects of active interest in evolutionary genetics for almost a century. However, to our knowledge, this problem has never been addressed directly, by considering the evolution of a gene, or group of genes, as a whole, including the complex effects of fitness interactions among multiple loci. Here, we use a precise model of protein fitness to compute the probability $P(s, \Delta t)$ that an allele, randomly sampled from a population at time t , has crossed a fitness valley of depth s during an interval $[t - \Delta t, t]$ in the immediate past. We study populations of model genes evolving under equilibrium conditions consistent with those in mammalian mitochondria. From this data, we estimate that genes encoding small protein motifs navigate fitness valleys of depth $2Ns \gtrsim 30$ with probability $P \gtrsim 0.1$ on a time scale of human evolution, where N is the (mitochondrial) effective population size. The results are consistent with recent findings for Watson–Crick switching in mammalian mitochondrial tRNA molecules.

Keywords: molecular evolution; epistasis; fitness valley crossing; thermodynamic stability

1. Introduction

The effect of a mutation on the fitness of an organism usually depends on the genetic background, or context in which it occurs, a phenomenon known as epistasis [1,2]. Because of this, the fitness landscape of a gene, a group of genes, or an organism will contain many isolated peaks and valleys [3,4], resembling the energy landscape of a physical system such as a glass. Under selection pressure, a population tends to evolve along a path of steepest ascent in fitness until it arrives in the neighborhood of a local fitness peak; In order to escape a sub-optimal fitness peak, the population, or some part of the population, must traverse across a valley of lower fitness. How such transitions occur [1,4–8], and how they relate to adaptation [9] have remained subjects of active interest in evolutionary genetics for almost a century.

The most basic example of valley crossing is realized in the compensatory interaction of individually deleterious mutations at two genetic loci – for instance, as might result from the physical interaction between amino acids in a protein, or a pair of nucleotides in an RNA molecule [5]. The archetypal model of this situation consists of a pair of diallelic loci with initial and final states AB and A'B' respectively; Mutations to A' and B' incur a fitness cost s relative to AB when introduced individually, but are neutral when introduced jointly. Kimura was the first to study this problem using the diffusion approach [5,10], and he found that deep fitness valleys could be crossed on a relatively short time scale if mutation rates are sufficiently large – specifically, when $2N\mu = 1$ where N is the population size and μ is the mutation rate per gene per generation. In this case, fitness valleys are navigated by a process known as stochastic tunneling [11], in which a small fraction of genes

35 accumulate in an intermediate state, are compensated by a second mutation, and ultimately proceed to
36 fixation – the intermediate acting as a kind of stepping stone [12]. The situation studied by Kimura
37 closely resembles the process of Watson–Crick switching between favorably paired nucleotides in
38 RNA stem sites, and in particular, switching in mammalian mitochondrial (mt) tRNA molecules where
39 stochastic tunneling is significant. Meer et al. investigated this problem somewhat recently [13], and,
40 using Kimura’s model, they found that mammalian mt tRNA switches may navigate valleys of depth
41 even as large as $2Ns \simeq 50$ (here, we assume that, for equal numbers of males and females, the effective
42 population size for mitochondrial genes is one fourth the effective population size for nuclear genes
43 [14,15]). In support of this result, Meer et al. obtain essentially the same estimate for $2Ns$ from the
44 frequency (p) of disrupted Watson–Crick pairs using the relation $p = \mu/s$ for mutation–selection
45 balance [16]. To put this number into context, it is at least ten times larger than would be expected if
46 the same model had evolved by sequential fixation of deleterious and compensatory mutations (i.e., as
47 would be expected when $\mu N \ll 1$ [17]).

48 While these estimates may be accurate, it is difficult to reconcile the evolutionary dynamics of
49 folded biomolecules with two–locus models. Naturally evolving genes encoding proteins and RNA
50 molecules are always faced with a complex spectrum of possible routes on their fitness landscapes,
51 and it is these spectra that ultimately determine the rate for crossing valleys of a given depth. Even for
52 tRNA molecules, compensation of disrupted Watson–Crick pairs seems to occur more often through
53 complex, indirect mechanisms than through direct compensation to restore Watson–Crick pairing [18].
54 Proteins are more connected objects than RNA molecules (i.e., with more opportunities for epistatic
55 interactions between loci), and the greater complexity of protein sequences is almost certain to present
56 a more complex spectrum of possible routes to a protein gene in which valleys (ravines, etc.) are
57 entered and exited in multiple steps (Figure A1).

58 Are the large effects predicted by Meer et al. common in biomolecular evolution? To our
59 knowledge, this kind of question has never been asked directly, by considering the problem of valley
60 crossing for a protein or RNA molecule as a whole, including the complex effects of fitness interactions
61 between multiple loci. Here, we simulate the evolution of a small protein motif using an exact fitness
62 model that is simple enough to allow for adequate sampling of valley crossing statistics. We evolve
63 populations of model genes by haploid Wright–Fisher dynamics across a range of mutation rates
64 spanning the sequential fixation ($\mu N \ll 1$) and stochastic tunneling ($\mu N \geq 1$) regimes, and we record
65 the mutational paths of all alleles in our populations. Using this data, we compute the probability
66 $P(s, \Delta t)$ that an allele, randomly sampled from a population at time t , has crossed a fitness valley of
67 depth s during a time interval $[t - \Delta t, t]$ in the immediate past. Surprisingly, we find that, even on
68 the time scale of human evolution, genes encoding small protein motifs evolving under conditions
69 consistent with mammalian mitochondria already navigate fitness valleys of depth $2Ns \gtrsim 30$ with
70 probability $P \gtrsim 0.1$, in rough agreement with the estimate for Watson–Crick switching in mt tRNAs
71 provided by Meer et al.

72 2. Methods

73 Epistatic effects play an essential part in protein evolution [19–24], and because these effects
74 depend on the relative probabilities of conformations in protein ensembles [25–27], it is important to
75 select a model in which the salient properties of protein ensembles are retained as much as possible.
76 Ultimately, we found that we could obtain sufficient data for valley crossing statistics in a reasonable
77 period of time using small lattice proteins. Lattice models have been used extensively in studies of
78 protein folding and evolution, and the model we employ here is similar to one recently used to explore
79 the effects of epistasis on the predictability of protein evolutionary pathways [25].

80 Below, we evolve lattice proteins under equilibrium conditions to maintain marginal stability in
81 a specific folded (native) conformation. The stability of a protein is measured, as usual, by the free
82 energy difference between the native conformation and the rest of the conformational ensemble,

$$\Delta G_N = E_N + \ln \left[-e^{-E_N} + \sum_{\gamma} e^{-E_{\gamma}} \right], \quad (1)$$

83 where E_{γ} is the energy of conformation γ , the subscript N denotes the native conformation, and factors
84 of temperature are absorbed into the definition of energy; The energy of a conformation is determined
85 from its amino acid contacts by empirical amino acid contact potentials [28] (as a result, energies are
86 defined in units of $RT \simeq 0.6$ kcal / mol).

87 We assume that mis-folded proteins are non-functional, and otherwise toxic to an organism
88 [29–31]. In this case, protein fitness can be defined by the probability of finding an individual protein
89 folded in its native conformation [25,32],

$$P_N = 1 / \left[1 + e^{\Delta G_N} \right]. \quad (2)$$

90 However, since most naturally occurring proteins are only marginally (as opposed to maximally) stable
91 [24], we decided to model fitness using a logistic function

$$w = 1 / \left[1 + e^{-k(P_N - 1/2)} \right] \quad (3)$$

92 where $k = 15$ (Figure S1). Under this condition, evolved genes in our simulations typically encode
93 proteins with $P_N > 0.75$ or, equivalently, $\Delta G_N < -1$ [33].

94 We evolve populations of protein genes by plain Wright–Fisher dynamics, with discrete
95 generations, fixed population size, and no recombination [34]. In each generation, a Poisson random
96 number of nucleotide sites with mean μN are selected at random; The sites are subjected to random
97 mutation, the fitness values of mutant alleles are computed, and N offspring are selected from the
98 population to form the next generation. The probability that an allele i survives to the next generation
99 is $p'_i = w_i p_i / \sum_j w_j p_j$, where p_i is the frequency of allele i in the current generation [35].

100 In the absence of recombination, each allele in a population has a unique mutational history
101 extending back to the origin of a simulation. To describe the statistics of valley crossing, we record
102 the histories of all alleles, and we compute $P(s, \Delta t)$, the probability that an allele, randomly sampled
103 from the population at time t , has crossed a fitness valley of depth s during the time interval $[t - \Delta t, t]$,
104 where time is measured in generations. Depending on its length, an interval $[t - \Delta t, t]$ along the fitness
105 history of an allele may contain a number of (perhaps nested) valleys of varying depth (Figure A1).
106 However, rather than attempt to record each valley as an individual event, we simply define s as
107 the maximum valley depth traversed along an interval (see Appendix). A peculiar feature of this
108 approach is that, for small values of s , we can choose an interval length Δt long enough that $P(s, \Delta t)$ is
109 a decreasing function of Δt (i.e., since larger values of s are more likely to occur on longer time scales).
110 However, below we will be concerned mainly with large values of s and time scales Δt that are far
111 from this sort of turnover region.

112 3. Results

113 To obtain data for $P(s, \Delta t)$ in a reasonable period of time, we limit our study to chains with at
114 most 16 amino acids (802, 075 conformations unrelated by symmetry [36]). The fitness landscapes of
115 longer chains will clearly differ, however, we expect that, within reason, results for somewhat longer
116 chains (e.g., 32 amino acids) will be similar, given proper adjustments to the mutation rate per gene μ
117 (see below).

118 We simulate protein evolution for different chain lengths ($L \leq 16$), native folds (Figures S2 and
119 S5), population sizes ($N \leq 10^3$), and mutation rates ($\mu N \leq 2$). In each situation, we conduct replicate
120 simulations in parallel on multiple processors of a high performance computer [37]. Each processor

121 begins with a monomorphic population constructed from N copies of a gene encoding a randomly
122 selected amino acid sequence. Each population is then equilibrated until an allele reaches fixation with
123 $P_N > 0.75$. After this point, alleles are sampled at random from a population every $64N$ generations
124 and their histories are recorded. For the most computationally intensive problems (i.e., for the largest
125 chain lengths and mutation rates), we are able to generate 10^5 samples in about ten days using 128
126 processors. For chains with 12 amino acids (15,037 conformations), samples can be obtained much
127 more rapidly, and results for chains of 12 and 16 amino acids are actually very similar (computer code
128 and sample data are available from the authors on request).

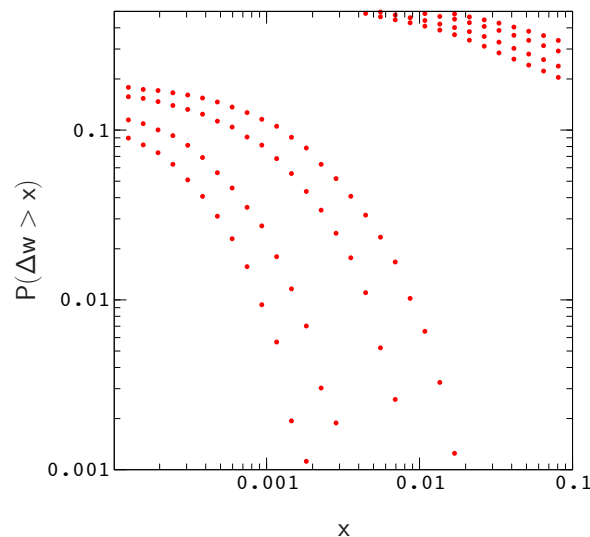


Figure 1. Distribution of beneficial fitness effects, $P(\Delta w > x)$. The distribution of deleterious fitness effects, $P(-\Delta w > x)$, is partially included in the upper right corner of the figure for reference. The plots are generated by randomly mutating evolved sequences sampled from simulations with $N = 100, 200, 500,$ and 1000 (the width of a plot increases with decreasing N). If the data for Δw in each plot is rescaled by the appropriate factor of N , the distributions $P(N\Delta w > x)$ roughly collapse to a single curve. For $N = 1000$, about 47 percent of the mutations are strongly deleterious ($N\Delta w < -5$), about 28 percent are nearly neutral ($-1 < N\Delta w < 1$), and about 0.7 percent are beneficial ($N\Delta w > 1$), consistent with results obtained by Tamuri et al. [38] for mammalian mitochondrial proteins (Tamuri et al. use logarithmic fitness differences in their work, however, this distinction can be neglected when $\ln(1+x) \simeq x$ [39]).

129 Since effective population size varies substantially across mammalian species, it is important to
130 ask whether simulations conducted for a particular population size can be used to estimate $P(s, \Delta t)$ for
131 larger (or smaller) populations evolving at the same overall rate μN , as expected from diffusion theory
132 [40]. To answer this question, we compared the scaled distributions $P(Ns > x, \Delta t)$ for population
133 sizes $N = 100, 200, 500$ and 1000 . For a fixed mutation rate μN , we find that plots of $P(Ns > x, \Delta t)$
134 roughly collapse to the same curve. As a result, we can estimate $P(s, \Delta t)$ for realistic populations using
135 a much smaller population size, which greatly reduces the amount of time spent on the simulations.
136 The reason for this is fairly simple – the local structure of the fitness landscape, as measured by e.g.
137 the distribution of fitness effects or the probability of compensatory neutral mutations, scales in a
138 similar way with population size; As population size increases, the landscape in the neighborhood of
139 an evolved sequence becomes less rugged in proportion to N .

140 Results of this exploration are described in Figures 1–2. In Figure 1, we plot the distributions
141 of beneficial and deleterious fitness effects, $P(\Delta w > x)$ and $P(-\Delta w > x)$, respectively. Each pair of
142 plots corresponds to a simulation for one of the population sizes listed above (the width of a plot

143 increases with decreasing N). The results describe proteins with 12 amino acids folding to the native
144 conformation in Figure S2, and the overall mutation rate in each simulation is $\mu N = 1$.

145 To generate data for Figure 1, we sampled the landscape around evolved genes using a simple
146 procedure that mimics error-prone polymerase chain reactions [41]; The procedure begins from a large
147 number of copies of an evolved gene. A Poisson random number of random mutations are applied
148 to each copy, and the results are sorted by the number of mis-sense mutations (i.e., neglecting back
149 mutations). For each simulation, we randomly selected 10^2 evolved sequences. Each evolved sequence
150 was then used to generate 10^4 random single amino acid mutants, for a total of 10^6 mutants per plot.

151 As is evident by closer inspection of Figure 1, the probability of a beneficial (or deleterious)
152 mutation with effect $\Delta w > x$ decreases almost linearly with increasing population size; The scaled
153 distributions $P(N\Delta w > x)$ for different population sizes roughly collapse onto a single curve. A
154 similar result is obtained for the distribution of compensatory neutral double mutants $P(s > x)$ (Figure
155 S3). The collapse is shown explicitly for the valley crossing probability $P(s > x, \Delta t)$ in Figure 2.

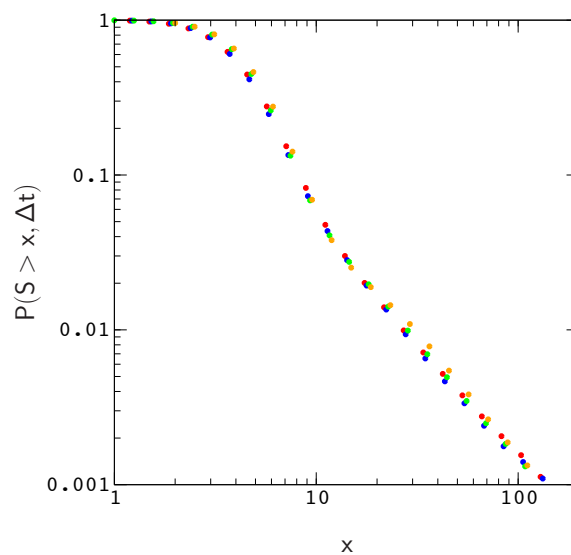


Figure 2. Probability, $P(S > x, \Delta t)$, that an allele, randomly sampled at time t , has crossed a valley of depth $S = 2Ns$ in the interval $[t - \Delta t, t]$ for $\Delta t = 128N$ and $\mu N = 1$. The data describe the same model as in Figure 1. Plots for population sizes $N = 100, 200, 500$, and 1000 are colored red, blue, green, and orange, respectively.

156 Given this result, we now restrict our attention to populations with $N = 200$ and proteins with
157 16 amino acids. To compare our results to those of Meer et al., we require the site mutation rate in
158 our model to agree with the pedigree rate for the control region in human mitochondria used in their
159 estimate for mammalian mt tRNA molecules – about 1×10^{-6} per site per year. Assuming a typical
160 length of about 80 nucleotides for tRNA molecules, a generation time of 20 years, and a (mitochondrial)
161 effective population size of $N = 2,500$, we arrive at an overall mutation rate of $\mu N \simeq 4$ for human mt
162 tRNA genes. To obtain the same site mutation rate for protein genes with 48 nucleotides (16 amino
163 acids), we need an overall mutation rate of about $\mu N \simeq 2$.

164 We plot $P(S > x, \Delta t)$ versus Δt for this situation in Figure 3, where $S = 2Ns$. The range of the
165 plot, $\Delta t \leq 128N$, roughly corresponds to the time scale of human evolution (about six million years).
166 Over this time scale, $P(S > x, \Delta)$ is roughly linear in Δt for $x \gtrsim 10$. The time scale for mammalian
167 evolution is much longer (on the order of tens of millions of years), however, on human time scales, the
168 frequencies of large events in our model are already approaching the ten percent levels observed for
169 Watson-Crick switching events in mammalian mt tRNA phylogenies [13]. For example, the probability

170 of sampling an allele that has crossed a fitness valley of depth $S > 9.1$ for $\Delta t = 128N$ is about 0.36, the
171 probability for $S > 17.8$ is about 0.07, and the probability for $S > 27.8$ is already about 0.03.

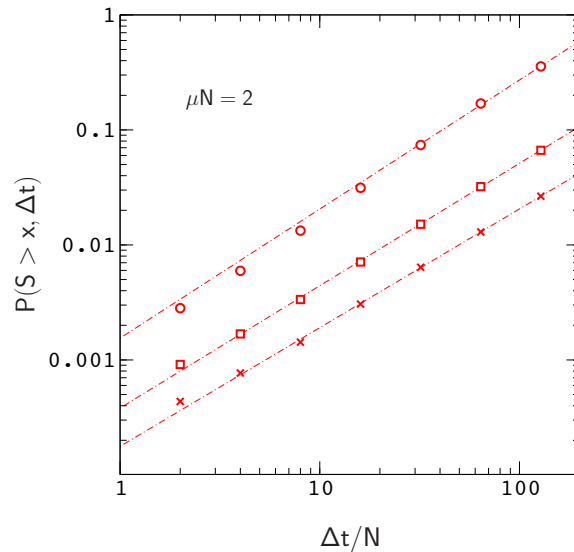


Figure 3. $P(S > x, \Delta t)$ versus Δt for $x \simeq 9.1$ (circles), 17.8 (squares) and 27.8 (crosses). The results describe proteins with 16 amino acids folding to the native conformation in Figure S5. Each data point is determined from over 10^5 allele histories. The range of the plot, $\Delta t \leq 128N$, corresponds to the time scale of human evolution (about six million years). The dashed lines (power law fits to the data) are very close to linear, increasingly so for larger values of x (see Appendix for more details).

172 Clearly, these numbers will continue to increase for larger values of Δt and larger mutation rates
173 μN (Figure 4). In addition, $P(S > x, \Delta)$ will also increase with chain length since, for a constant site
174 mutation rate, the mutation rate per gene μ is proportional to chain length. If we assume that the
175 fitness landscapes of proteins with 16 amino acids can be used to represent the landscapes of larger
176 chains, then e.g. doubling the mutation rate per gene will have the same effect as doubling the chain
177 length to obtain a protein encoded by the same amount of genetic material as a tRNA molecule or
178 small protein motif [42]. This is not an unreasonable assumption, since, as we have noted earlier (see
179 the captions to Figures 1 and S3), the local structures of fitness landscapes in the model, as measured
180 by the scaled distribution functions $P(N\Delta w > x)$ and $P(Ns > x)$, are already similar to those inferred
181 from real proteins with much longer sequences. In this case, extrapolating from the data in Figure 4,
182 we find that the probability of sampling an allele that has crossed a valley of depth $S > 27.8$ over a
183 time interval $\Delta t = 128N$ increases to about $P \simeq 0.1$. Thus, even neglecting the anticipated increase in
184 $P(S > x, \Delta)$ for $\Delta t > 128N$, the results for small protein motifs are already consistent with those of
185 Meer et al.

186 As a final note, it is important to remark that the deepest valleys navigated by alleles in our
187 simulations actually correspond to events in which a deleterious mutation is, to a major extent,
188 compensated by a mutation back to a similar amino acid type at the same site (see Figure S6). It is also
189 worth noting that local fitness peaks sampled at various points in our simulations (by steepest ascent
190 in fitness, starting from a randomly sampled sequence) are often separated by deep fitness valleys, or
191 ravines.

192 4. Discussion

193 Does the model provide an accurate picture of fitness valley crossing for small protein motifs?
194 This question is very difficult to answer due to the extreme complexity of protein fitness landscapes,
195 and the unknown effects of varying host genetic backgrounds experienced by protein genes. However,

196 from basic principles, it appears that the model is roughly accurate: Local features of protein fitness
197 landscapes, such as the distribution of fitness effects, can be inferred from protein sequences by fitting
198 a population dynamics model to branches of a phylogenetic tree [38] such that background effects are
199 accounted for by allowing the parameters of the model to vary among branches. Tamuri et al. have
200 used this type of approach to estimate the distribution of fitness effects for mammalian mitochondrial
201 proteins [38], and our results for $P(N\Delta w > x)$ are in good agreement with their data (Figure 1). Given
202 the similar nature of fitness conditions in each system (i.e., that proteins are also polymers required to
203 fold into a specific shape in order to function), it seems reasonable to expect that the topographies of
204 model fitness landscapes resemble those of small protein motifs.

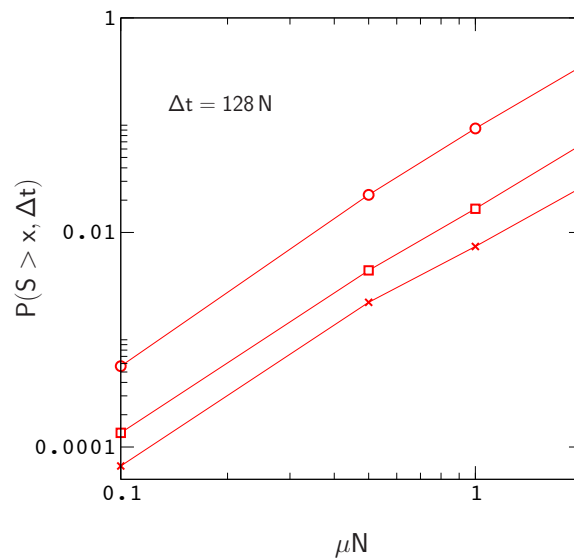


Figure 4. $P(S > x, \Delta t)$ versus μN for $x \simeq 9.1$ (circles), 17.8 (squares) and 27.8 (crosses). The results describe the same simulation data as Figure 3.

205 Longer chains with more developed core structures, and more restrictive fitness conditions such
206 as binding to proteins within a larger domain, may lead to qualitatively different results due to the
207 potential for larger compensatory effects [27], and the suppression of substitution rates in the core and
208 binding interface regions. In addition, much larger mutation rates can occur in micro-organisms such
209 as viruses [43], and our results suggest that, under these conditions, fitness valley crossing will be more
210 pronounced. RNA viruses such as HIV-1 are also subject to high rates of recombination [44,45], which
211 may interfere with valley crossing [5,6]. Because the computational cost of our simulations increases
212 in proportion to the number of mutations (i.e., the number of fitness calculations), a full study of the
213 model for virus proteins may be challenging. However, we hope to address these problems in future
214 work.

215 **Supplementary Materials:** The following are available online at <http://www.mdpi.com/2073-4425/xx/1/5/s1>,
216 Figure S1: Plot of the logistic fitness function defined in Equation (3); Figure S2: Native fold studied in Figures 1–2;
217 Figure S3: Plot of $P(s > x)$ for the native fold studied in Figures 1–2; Figure S4: Plot of $P(S > x)$ for an inferred
218 Potts model of cytochrome c oxidase subunit 2; Figure S5: Native fold studied in Figures 3–4; Figure S6: Plot of
219 $P(S > x, \Delta t)$ for the subset of deleterious mutations compensated by a mutation back to a similar amino acid type
220 at the same site.

221 **Author Contributions:** Conceptualization, Erik Nelson; Funding acquisition, Nick Grishin; Investigation, Erik
222 Nelson; Software, Erik Nelson; Supervision, Nick Grishin.

223 **Funding:** This research was funded in part by a grant from the National Institutes of Health GM127390 to NVG.

224 **Acknowledgments:** It is a pleasure to thank Daniel Moser for help with the computations, and two anonymous
225 reviewers for helpful suggestions.

226 **Conflicts of Interest:** The authors declare no conflict of interest.

227 **Appendix**

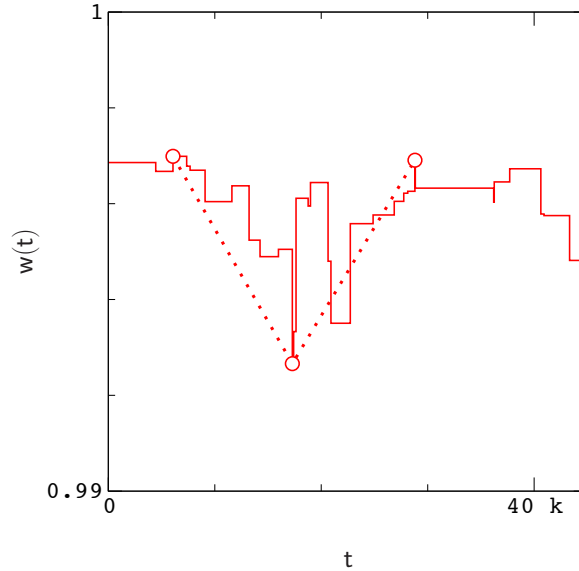


Figure A1. Fitness history of an allele between adjacent fixation events (solid line) sampled from a simulation with $N = 10^3$ and $\mu N = 1$. Circles and dashed lines indicate the configuration of points which maximize the valley depth $s = \min\{w_i - w_j, w_k - w_j\}$.

228 To compute the maximum valley depth traversed along an interval (Figure A1), we consider all
 229 possible placements of three points, w_i , w_j and w_k , where $i < j < k$ denote the occurrence times of
 230 mutations. For a given placement of points, valley depth s is defined as the smaller of the two fitness
 231 differences $w_i - w_j$ or $w_k - w_j$. The maximum valley depth can then be expressed as,

$$\mathbf{max} s = \mathbf{max}_{i < j < k} [\mathbf{min}\{w_i - w_j, w_k - w_j\}]. \quad (\text{A1})$$

232 To avoid complicating our expressions, we use the plain symbols s and $S = 2Ns$ to denote maximum
 233 valley depth in $P(s > x, \Delta t)$ and $P(S > x, \Delta t)$.

234 The structure of $P(S > x, \Delta t)$ can be explained roughly as follows: As we noted earlier, an interval
 235 $[t - \Delta t, t]$ along a fitness trace may contain a number of distinct valleys of varying depth. Valleys
 236 of large depth are rare on the time scale of human evolution and short lived. As a result, when x is
 237 large, doubling Δt doubles the probability that a valley with depth greater than x will occur within an
 238 interval $[t - \Delta t, t]$, and $P(S > x, \Delta t)$ increases linearly with Δt . This will be true as long as Δt is not
 239 too large or too small; For large enough Δt , $P(S > x, \Delta t)$ will begin to saturate (i.e., $P \rightarrow 1$), at which
 240 point the slope of the curve, $\partial P(S > x, \Delta t) / \partial \Delta t$, tends to zero, and linearity is lost. Conversely, for
 241 small enough Δt , the typical duration of an event (valley of depth greater than x) will begin to exceed
 242 Δt , and again $\partial P(S > x, \Delta t) / \partial \Delta t$ will begin to change. This change will depend both on x and the
 243 topography of valleys with depth greater than x , however, we have not explored this issue in detail.

244 References

- 245 1. Phillips, P.C. Epistasis – the essential role of gene interactions in the structure and evolution of genetic
246 systems. *Nature Reviews Genetics* **2008**, *9*, 855–867.
- 247 2. Starr, T.N.; Thornton, J.W. Epistasis in protein evolution. *Protein Sci.* **2016**, *25*, 1204–1218.
- 248 3. Wright, S. The roles of mutation, inbreeding, cross–breeding and selection in evolution. Proceedings of the
249 sixth international congress of genetics; Jones, D.F., Ed. Brooklyn Botanic Garden, Menasha, WI, 1932, pp.
250 356–366.
- 251 4. Johnson, N. Sewall Wright and the Development of Shifting Balance Theory. *Nature Education* **2008**, *1*, 52.
- 252 5. Kimura, M. The role of compensatory neutral mutations in molecular evolution. *J. Genetics* **1985**, *64*, 7–19.
- 253 6. Weinreich, D.M.; Chao, L. Rapid evolutionary escape by large populations from local fitness peaks is likely
254 in nature. *Evolution* **2005**, *59*, 1175–1182.
- 255 7. van Nimwegen, E.; Crutchfield, J.P. Metastable evolutionary dynamics: crossing fitness barriers or escaping
256 via neutral paths? *Bull. Math. Biol.* **2000**, *62*, 799–848.
- 257 8. Burton, O.J.; Travis, J.M.J. The Frequency of fitness peak shifts is increased at expanding range margins
258 due to mutation surfing. *Genetics* **2008**, *179*, 941–950.
- 259 9. Arias, M.; le Poul, Y.; Chouteau, M.; Boisseau, R.; Rosser, N.; Thery, M.; Llaurens, V. Crossing fitness valleys
260 : empirical estimation of a fitness landscape associated with polymorphic mimicry. *Proc. R. Soc. B* **2016**,
261 *283*, 20160391.
- 262 10. Kimura, M. Diffusion models in population genetics. *J. Appl. Prob.* **1964**, *1*, 177–232.
- 263 11. Iwasa, Y.; Michor, F.; Nowak, M.A. Stochastic tunnels in evolutionary dynamics. *Genetics* **2004**,
264 *166*, 1571–1579.
- 265 12. Covert III, A.W.; Lenski, R.E.; Wilke, C.O.; Ofria, C. Experiments on the role of deleterious mutations as
266 stepping stones in adaptive evolution. *Proc. Natl. Acad. Sci. USA* **2013**, *110*, E3171–E3178.
- 267 13. Meer, M.V.; Kondrashov, A.S.; Artzy-Randrup, Y.; Kondrashov, F.A. Compensatory evolution in
268 mitochondrial tRNAs navigates valleys of low fitness. *Nature* **2010**, *464*, 279–283.
- 269 14. Osada, N.; Akashi, H. Mitochondrial–nuclear interactions and accelerated compensatory evolution :
270 evidence from the primate cytochrome c oxidase complex. *Mol. Biol. Evol.* **2012**, *29*, 337–346.
- 271 15. Charlesworth, B. Effective population size and patterns of molecular evolution and variation. *Nat. Rev.*
272 *Genet.* **2009**, *10*, 195–205.
- 273 16. Haldane, J.B.S. The effect of variation on fitness. *Am. Nat.* **1937**, *71*, 337–349.
- 274 17. McCandlish, D.M.; Stoltzfus, A. Modeling evolution using the probability of fixation : history and
275 implications. *Q. Rev. Biol.* **2014**, *89*, 225–252.
- 276 18. Kern, A.D.; Kondrashov, F.A. Mechanisms and convergence of compensatory evolution in mammalian
277 mitochondrial tRNAs. *Nature Genetics* **2004**, *36*, 1207–1212.
- 278 19. Breen, M.S.; Kremena, C.; Vlasov, P.K.; Notredame, C.; Kondrashov, F.A. Epistasis as the primary factor in
279 molecular evolution. *Nature* **2012**, *490*, 535–538.
- 280 20. McCandlish, D.M.; Rajon, E.; Shah, P.; Ding, Y.; Plotkin, J.B. The role of epistasis in protein evolution.
281 *Nature* **2013**, *497*, E1–E2.
- 282 21. Breen, M.S.; Kremena, C.; Vlasov, P.K.; Notredame, C.; Kondrashov, F.A. Breen et al. reply. *Nature* **2013**,
283 *497*, E2–E3.
- 284 22. Starr, T.N.; Flynn, J.M.; Mishra, P.; Bolon, D.N.A.; Thornton, J.W. Pervasive contingency and entrenchment
285 in a billion years of Hsp90 evolution. *Proc. Natl. Acad. Sci* **2018**, *115*, 4453–4458.
- 286 23. Otwinowski, J.; McCandlish, D.M.; Plotkin, J.B. Inferring the shape of global epistasis. *Proc. Natl. Acad. Sci.*
287 *USA* **2018**, *115*, E7550–E7558.
- 288 24. Posfai, A.; Zhou, J.; Plotkin, J.B.; Kinney, J.B.; McCandlish, D.M. Selection for protein stability enriches for
289 epistatic interactions. *Genes* **2018**, *9*, 423–432.
- 290 25. Sailer, Z.R.; Harms, M.J. Molecular ensembles make evolution unpredictable. *Proc. Natl. Acad. Sci. USA*
291 **2017**, *114*, 11938–11943.
- 292 26. Noivirt-Brik, O.; Unger, R.; Horovitz, A. Analyzing the origin of long–range interactions in proteins using
293 lattice models. *BMC Struct. Biol.* **2009**, *9*, 4.
- 294 27. Nelson, E.D.; Grishin, N.V. Long–range epistasis is mediated by structural change in a model of ligand
295 binding proteins. *PLoS ONE* **2016**, *11*, e0166739.

- 296 28. Miyazawa, S.; Jernigan, R.L. Residue–residue potentials with a favorable contact pair term and an
297 unfavorable high packing density term for simulation and threading. *J. Mol. Biol.* **1996**, *256*, 623–644.
- 298 29. Serohijos, A.W.R.; Rimas, Z.; Shakhnovich, E.I. Protein biophysics explains why highly abundant proteins
299 evolve slowly. *Cell Reports* **2012**, *2*, 249–256.
- 300 30. Serohijos, A.W.R.; Lee, S.Y.R.; Shakhnovich, E.I. Highly abundant proteins favor more stable 3D structures
301 in yeast. *Biophys. J.* **2013**, *104*, L01–L03.
- 302 31. Drummond, D.A.; Wilke, C.O. Mistranslation–induced protein misfolding as a dominant constraint on
303 coding–sequence evolution. *Cell* **2008**, *134*, 341–352.
- 304 32. Goldstein, R.A. The evolution and evolutionary consequences of marginal thermostability in proteins.
305 *Proteins* **2011**, *79*, 1396–1407.
- 306 33. Bloom, J.D.; Silberg, J.J.; Wilke, C.O.; Drummond, D.A.; Adami, C.; Arnold, F.H. Thermodynamic prediction
307 of protein neutrality. *Proc. Natl. Acad. Sci. USA* **2005**, *102*, 606–611.
- 308 34. Gillespie, J.H. *Population genetics*; Johns Hopkins University Press: Baltimore, MD, 2004.
- 309 35. Tachida, H. Molecular evolution in a multisite nearly neutral mutation model. *J. Mol. Evol.* **2000**, *50*, 69–81.
- 310 36. Slade, G. Self–avoiding walks. *Math. Intel.* **1994**, *16*, 29–35.
- 311 37. UT Southwestern Medical Center BioHPC. <https://portal.biohpc.swmed.edu/content/>.
- 312 38. Tamuri, A.U.; dos Reis, M.; Goldstein, R.A. Estimating the distribution of selection coefficients from
313 phylogenetic data using sitewise mutation–selection models. *Genetics* **2012**, *190*, 1101–1115.
- 314 39. Nelson, E.D.; Grishin, N.V. Inference of epistatic effects in a key mitochondrial protein. *Phys. Rev. E* **2018**,
315 *97*, 062404.
- 316 40. Felsenstein, J. Theoretical population genetics. [https://http://evolution.gs.washington.edu/pgbook/
317 pgbook.pdf](https://http://evolution.gs.washington.edu/pgbook/pgbook.pdf), 2016. See Box 3, p. 340.
- 318 41. Sarkisyan et al., K.S. Local fitness landscape of the green fluorescent protein. *Nature* **2016**, *533*, 397–401.
- 319 42. Jäger, M.; Zhang, Y.; Bieschke, J.; Nguyen, H.; Dendle, M.; Bowman, M.E.; Noel, J.P.; Gruebele, M.;
320 Kelly, J.W. Structure–function–folding relationship in a WW domain. *Proc. Natl. Acad. Sci. USA* **2006**,
321 *103*, 10648–10653.
- 322 43. Wilke, C.O. Molecular clock in neutral protein evolution. *BMC Genetics* **2004**, *5*, 25.
- 323 44. Bonhoeffer, S.; Chappey, C.; Parkin, N.T.; Whitcomb, J.M.; Petropoulos, C.J. Evidence for positive epistasis
324 in HIV–1. *Science* **2004**, *306*, 1547–1550.
- 325 45. Moradigaravand, D.; Kouyos, R.; Hinkley, T.; Haddad, M.; Petropoulos, C.J.; Engelstädter, J.; Bonhoeffer, S.
326 Recombination accelerates adaptation on a large–scale empirical fitness landscape in HIV–1. *PLoS Genetics*
327 **2014**, *10*, e1004439.